Rates of occurrence of TIGER HF radar echo parameters sorted according to the *Kp* index and the interplanetary magnetic field (IMF) – early results

M. L. Parkinson[1], J. C. Devlin[2], M. Pinnock[3], P. R. Smith[2], P. L. Dyson[1], and C. L. Waters[4]

[1]Department of Physics, La Trobe University, Bundoora Campus, Victoria 3083, Australia; m.parkinson@latrobe.edu.au

[2]Department of Electronic Engineering, La Trobe University, Bundoora Campus, Victoria 3083, Australia; j.devlin@ee.latrobe.edu.au

[3]British Antarctic Survey, Natural Environment Research Council, High Cross, Madingley Road, Cambridge, CB3 0ET, UK; mpi@pcmail.nerc-bas.ac.uk

[4]Applied Physics Laboratory, Johns Hopkins University, 11100 Johns Hopkins Rd., Laurel, MD, 20723-6099, USA; physpuls8@cc.newcastle.edu.au

Introduction

The recently commissioned Tasman International Geospace Environment Radar (TIGER) began scientific observations in December 1999. TIGER is located in a near sea-level wetland on Bruny Island, off the southern tip of Tasmania, Australia. Geographically, it is the most equatorward of any of the SuperDARN radars (43.4° S, 147.2° E), yet the default range gate (180 to 3555 km) covers the interval of altitude adjusted corrected geomagnetic latitude (AACGM) 57° S to 88° S. This is because the AACGM pole is tilted toward the equator near the longitude of TIGER beam 4, which is closely aligned with the magnetic meridian. Thus the radar observes a geomagnetic high-latitude region of the ionosphere subjected to stronger insolation and mid-latitude neutral dynamics than any other radar in the network.

Moreover, TIGER has another outstanding feature: the bore sight of the normal 16-beam scan is geographically due south across the Southern Ocean. Most of the first-hop "ground" echoes are actually backscatter from some of the largest ocean waves on the planet, thus ensuring the viability of the radar for remote sensing of surface winds and sea state.

In this paper we present basic occurrence statistics of FITACF parameters derived from all the normal scan beam #4 observations made during December 1999 to February 2000. This interval corresponds to an austral summer, sunspot maximum data set. The results are sorted according to the *Kp* index and the IMF vector separated into the four basic quadrants of the (*By*, *Bz*) plane.

Results

During summer it was found that 65% of the echoes detected by TIGER were sea echoes, mostly observed via first-hop *F*-region propagation. Figure 1 shows that the peak occurrence rate was >80% near to 19 h LT. The echoes mostly observed during ~05 to 11 h MLT at ranges less than 500 km were also probably sea echoes observed via sporadic *E*-layer propagation. However, some of the echoes may have been associated with the radar wave vector achieving normal incidence with meteor trails.

Figure 2 shows that the majority of the remaining echoes flagged as "ionospheric" were 1/2- and 1 1/2-hop backscatter from decameter-scale irregularities in the nightside auroral oval. Although the zero angle-of-arrival found for 3% of TIGER echoes may be erroneous, their values imply a small population of surface-wave sea echoes (ranges <500 km), and direct line-of-sight ionospheric echoes. Figure 2 shows the peak occurrence rate of *F*-region ionospheric echoes was ~70% near 0130 MLT and 71° S (magnetic latitudes hereafter) for all *Kp* values. Supplementary figures found in the appendix show that this peak moved equatorward with increasing *Kp*. However, the total number of echoes detected decreased dramatically with *Kp*, thereby demonstrating the sensitivity of the experiment to enhanced ionospheric absorption. Moreover, there was usually a distinct minimum occurrence just past local solar noon, consistent with the normal diurnal variation of *D*-region absorption at mid-latitudes.

Lastly, Figure 2 also reveals a population of echoes found mostly between midnight and noon and the first 600 km of range, but peaking at 5 h MLT and ranges 300– 400 km. These limits are some of the well-known characteristics of meteor echoes observed using the other SuperDARN radars [1].

Figure 3 shows the statistical average line-of-sight *F*-region velocities for all values of *Kp*. Convection velocities given by the IZMIRAN electrodynamic convection model (IZMEM) [2] were superimposed using thin-black lines with lengths proportional to the magnitude of the modeled velocities. There is clear evidence in the observations for the dawn and dusk convection cells, and the cross polar cap jet. Supplementary figures found in the appendix show that the cross polar cap jet was least developed for *By* negative and *Bz* positive, and most developed for *By* positive and *Bz* negative, consistent with the prediction of statistical convection models including IZMEM. However, the TIGER observations suggest that the IZMEM dawn convection cell should be rotated by ~01 h in MLT toward magnetic midnight.

Figure 4 shows the statistical average *F*-region spectral widths for all values of *Kp*. These results are especially interesting. First, the location of the greater cusp/cleft is obvious from the maximum spectral widths observed in the pre-noon sector near 78° S magnetic. However, of greater interest is the sharp decrease in spectral width on the nightside at ~67° S. This feature is coincident with a sharp decrease in cross polar cap velocity shown in Figure 3 and is tentatively associated with the equatorward limit of magnetospheric convection. This feature also formed the poleward wall of a "trough" in spectral widths (~80 m s^{-1}) found between ~62° S and 67° S, and lasting from ~1930 to 0300 MLT. A region of enhanced spectral widths (150 to > 250 m s^{-1}) found between ~60° S and 64° S then occurred during ~0300 to 0600 MLT. This last feature is not meteor scatter, and is unexplained at the time of writing.

Conclusions

Our initial impressions are that the occurrence rates of TIGER ionospheric and sea echoes are higher than that observed by other SuperDARN radars. Moreover, the observed line-of-sight *F*-region velocities are basically consistent with dominant features in statistical convection models. These results help to validate the successful construction, installation, and operation of TIGER. In fact, the high occurrence rates of TIGER echoes supports the ray-tracing results that suggest SuperDARN radars would detect more echoes if they were located equatorward of their present locations.

It is important to consider the major factors determining when echoes from decameter-scale irregularities are observed including the availability of suitable propagation modes, the diurnal variation of ionospheric absorption, and the irregularity production mechanisms. Unfortunately, as with other radars in the SuperDARN network the number of ionospheric echoes detected by TIGER rapidly diminished with increasing geomagnetic activity. Moreover, relatively few cusp-like echoes were seen because of its great range and enhanced *D*-region absorption in the dayside ionosphere.

An interesting feature in the present results was the sharp decrease in line-of-sight *F*-region velocity and spectral width at ~67° S. This feature is tentatively associated with the poleward wall of the main ionospheric trough and the subsequent trough in spectral widths with the overall extent of the trough. Our interpretation begs the question as to why the spectral widths subsequently increase again at the equatorward boundary of this feature. Moreover, is there any association between this feature and other signatures of the plasmapause? Lastly, the region of enhanced spectral widths occurring during ~0300 to 0600 MLT may be associated with *F*-region irregularities forming high in the pre-sunrise trough when the electron densities are lowest. Of course, all of these results are very early and subject to clarification in the near future.

References

[1] Hall, G. E., et al., *J. Geophys. Res.*, **102**, 14,603-14,614, 1997.

[2] Papitashvili, V. O., et. al., *J. Geophys. Res.*, **99**, 13,251-13,262, 1994.

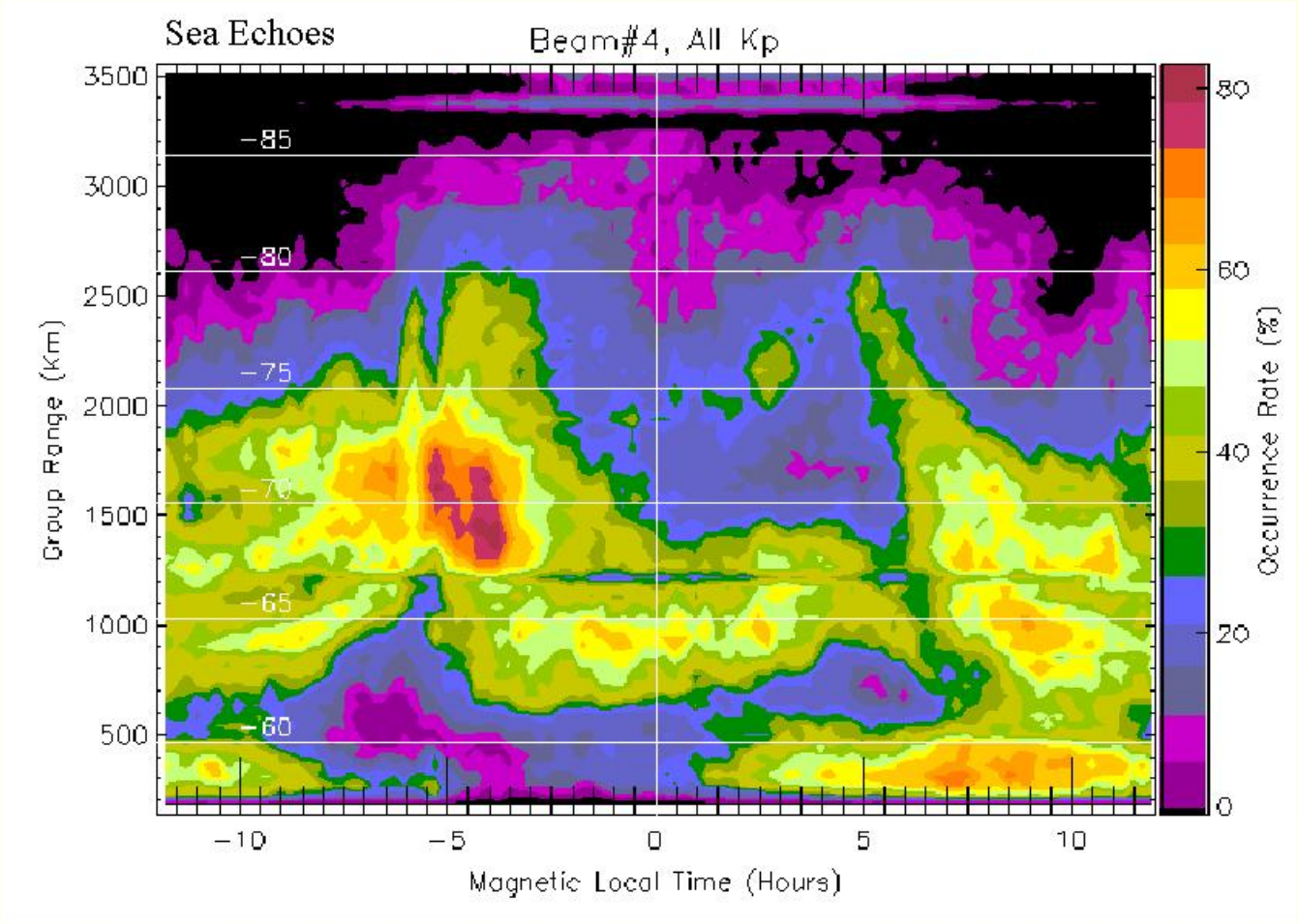

Figure 1: *Rectangular contour plot of the occurrence rate of sea echoes detected on TIGER beam 4 for all values of Kp during December 1999 to February 2000. The occurrence rate was calculated for each bin of 15 minutes in magnetic local time (MLT) and each range separated by 45 km. AACGM latitudes are superimposed in white and tick marks on the abscissa are at 30-minute intervals.*

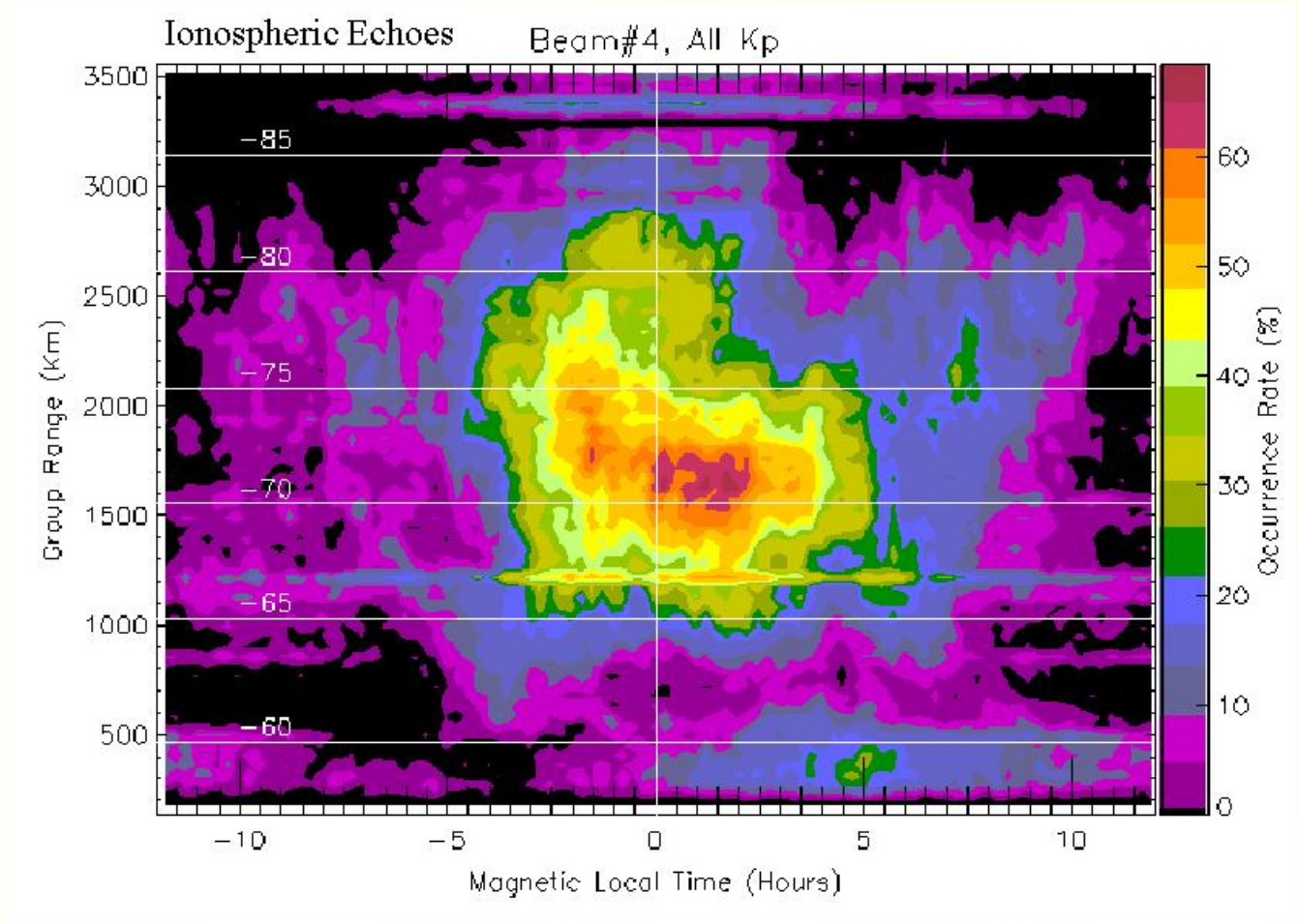

Figure 2: *Rectangular contour plot of the occurrence rate of ionospheric echoes detected on TIGER beam 4 for all values of Kp during December 1999 to February 2000. Otherwise the format of the figure is the same as Figure 1.*

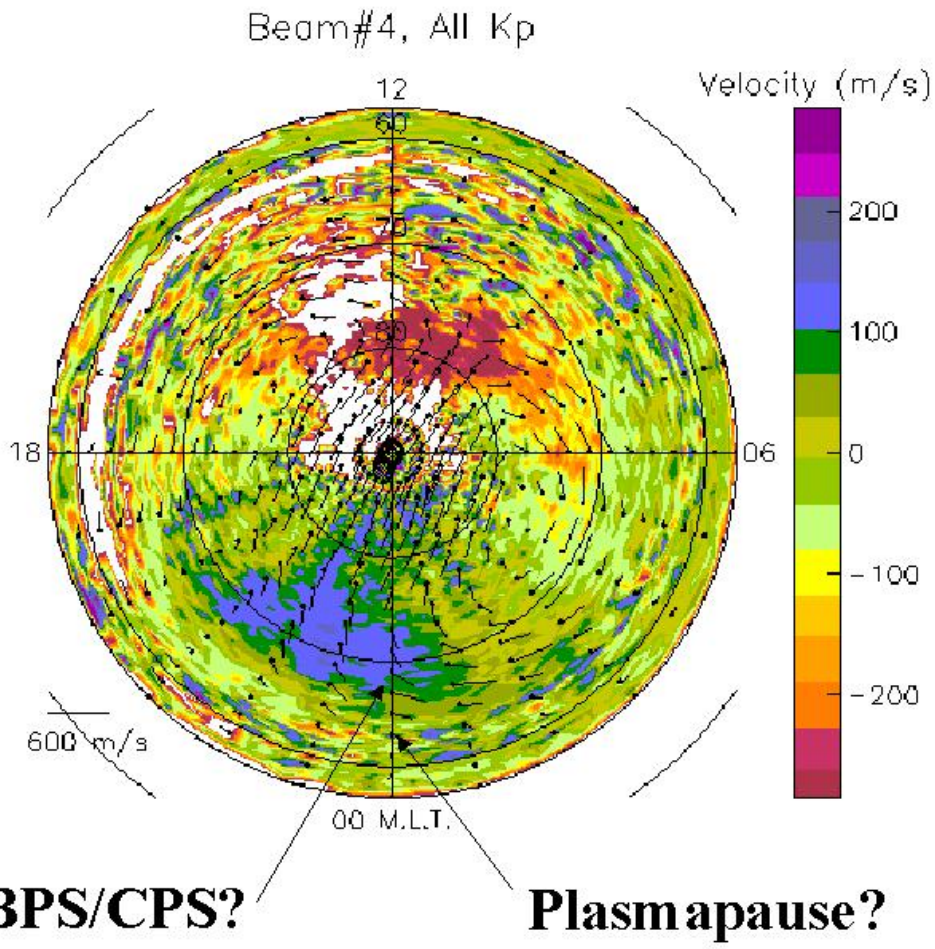

Figure 3: *Clock dial contour plot of the statistical average line-of-sight Doppler velocities measured on TIGER beam 4 for all values of Kp during December 1999 to February 2000. An average velocity was calculated for each bin of 15 minutes in magnetic local time (MLT) and each range separated by 45 km. The four black circles superimposed on the plot correspond to AACGM latitudes of 57° , 60° , 70° and 80° S. Probable midnight locations of the boundary between the ionospheric projection of the Boundary Plasma Sheet (BPS) and the Central Plasma Sheet (CPS) (i.e., near the poleward wall of the main ionospheric trough), and the plasmapause, are indicated.*

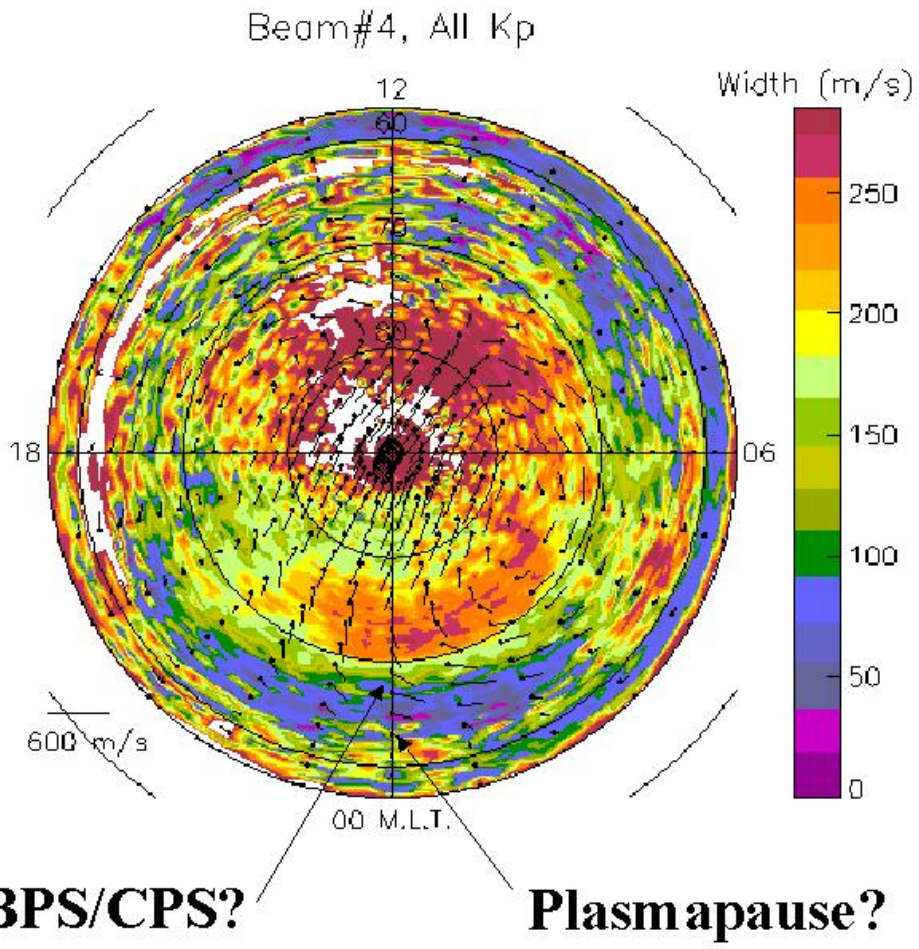

Figure 4: *Clock dial contour plot of the statistical average Doppler velocity widths measured on TIGER beam 4 for all values of Kp during December 1999 to February 2000. Otherwise the format of the figure is the same as Figure 3.*